

Determination of nanomolar dissolved polycyclic aromatic hydrocarbons in different water and wastewater samples using a metal-organic framework-199@graphene oxide fiber and headspace solid-phase microextraction

Fatemeh Kardani^a, Roya Mirzajani^{a,*}, Zahra Ramezani^b

^aChemistry Department, College of Science, Shahid Chamran University of Ahvaz, Ahvaz, Iran, Tel./Fax: +986133738044; emails: rmirzajani@scu.ac.ir (R. Mirzajani), kardanifateme@yahoo.com (F. Kardani)

^bDepartment of Medicinal Chemistry, School of Pharmacy, Ahvaz Jundishapur University of Medical Sciences, Ahvaz, Iran, email: zramezani@yahoo.com

Received 6 February 2018; Accepted 18 November 2018

ABSTRACT

A hybrid coating material composed of the metal-organic framework-199 and graphene oxide has been synthesized and coated on stainless steel fiber in a simple manner, characterized, and used in a fiber headspace solid-phase microextraction (HS-SPME) method in combination with gas chromatography-flame ionization detection. The synthesized fiber exhibited high sensitivity toward microextraction of polycyclic aromatic hydrocarbons (PAHs). The fibers were characterized using Fourier transform infrared spectrometer, scanning electron microscopy, and X-ray diffraction. Optimization of the microextraction conditions for the HS-SPME method was accomplished using a response surface design of Box–Behnken. Under optimized conditions, good linearity for the analytes was obtained in the range of 0.1–200.0 μgL^{-1} , with the limits of detection ($S/N = 3$) ranging from 0.027 to 0.041 μgL^{-1} . The interday and intraday relative standard deviations for various PAHs at three different concentration levels ($n = 5$) using a single fiber were 1.6%–2.3%. The method was successfully applied for quantification of naphthalene, phenanthrene, anthracene, and chrysene in industrial wastewater and environmental water samples with the recoveries between 93% and 103%.

Keywords: PAHs; Headspace microextraction; Metal-organic framework; GC-FID; Design of experiment; Adsorption

1. Introduction

Polycyclic aromatic hydrocarbons (PAHs) are a vast class of ubiquitous and toxic compounds, including two or more aromatic rings, originated through incomplete combustion or pyrolysis of organic matters such as oil, fossil fuels, wood, or coal [1]. Therefore, they belong to the group of common environmental pollutants of both natural and anthropogenic origins [2]. The monitoring of PAHs has become a serious problem due to their well-known carcinogenic and mutagenic effects [3]. Moreover, it has recently been observed that PAHs interfere with the hormone system of the human body and may have effects on reproduction [4]. These substances

can be found in a number of different types of samples, both biological and environmental. Water can contain substantial amounts of PAHs that have leached from the soil or they can also enter into water from industrial effluents and accidental spills during oil transfer by sea.

However, testing the aquatic toxicity of PAHs and their mixtures at well-defined exposure concentrations can be difficult because PAHs are poorly soluble in water and are easily lost by volatilization and sorption [5]. As PAHs were monitored in the environment, especially in aqueous media at trace and ultra trace levels, more effective preconcentration methods are required, and the development of effective extraction and enrichment techniques for PAHs to be applied

* Corresponding author.

prior to an analytical procedure is, therefore, necessary [6]. In this regard, various analytical methodologies have been applied for the sample pretreatment and preconcentration of PAHs including solid-phase extraction [7], liquid-liquid extraction [8], dispersive liquid-liquid microextraction [9], and solid-phase microextraction (SPME) [10].

At the present time, SPME is perhaps the most effective technique employed for the extraction and enrichment of volatile and semivolatile compounds at trace and ultra trace amounts in different matrices. The SPME technique is extremely attractive because it is easy to operate. It combines the extraction and preconcentration steps of analytes into a single process and enables direct elution at chromatographic system for analysis. Further advantages of SPME compared with other methods of sample pretreatment are the reusability of the fiber, the portability of the system, minimal contamination and loss of the sample at transport and storage, and, finally, the existence of numerous extraction phases in the literature [11]. SPME is indeed an equilibrium microextraction technique rather than an exhaustive extraction method; that is, the extraction efficiency is measured using the distribution of the target compounds between the sample matrix and the fiber coating. Therefore, the most critical part of the SPME device is the coating itself [12].

However, currently, the number and variety of commercially available SPME coatings are still limited [13]. To solve this problem, various novel homemade SPME coating materials, including carboxylated solid carbon spheres [14], polymeric ionic liquids [15], multiwalled carbon nanotube (MWCNT) composite [16], graphene and graphene-based materials [17], periodic mesoporous organosilica materials [18], and molecular imprinted monolithic fibers [19], have been synthesized as SPME fiber coatings.

In recent years, fragile commercial fused silica fiber has been replaced by stainless steel wire because of its lower price and greater mechanical stability [20]. Furthermore, the growth of coating materials has also been extensive.

Metal-organic frameworks (MOFs) are a fascinating group of zeolite-like compounds synthesized by metal ions or clusters chelating with organic ligands. On the basis of the availability of diverse metal ions, organic ligands, and the chelating ratio difference, MOFs of numerous structures have demonstrated excellent properties of different structures, such as tunable pore sizes and large surface areas [21,22].

However, most MOFs have some drawbacks, including poor chemical stability, which must be overcome if they are to find practical utility under industrial conditions [23]. Recently, considerable body of research has indicated that combining MOFs with different functional materials such as carbon nanotubes, graphene oxide (GO), graphite oxide, and carbon nanofibers to prepare different composites can significantly and remarkably enhance the performance of MOFs [24]. GO, prepared by oxidation of graphite with strong oxidizing agents, consists of distorted graphene layers bearing carbonyl, hydroxyl, and epoxy groups on the basal planes and carboxylic functionality on the edges of the carbon sheets [25,26]. Owing to its chemical structure, GO has been utilized in the preparation of various kinds of composite materials with better electronic and adsorptive properties [27].

In this study, we used MOF-199/GO composite coating on the surface of stainless steel wire as a fiber coating in SPME for the microextraction of PAHs with a gas chromatograph

equipped with a flame ionization detector. Recently, chemometrics method has been frequently used for analytical technique optimization problems [28]. Among the advantages of applying the mentioned methods is the reduction in the number of experiments, resulting in lower reagent consumption and considerably less laboratory work [29]. These methods provide the simultaneous study of multiple control factors and the development of mathematical models that permit the assessment of the relevance and statistical significance of the factors being studied. They also simplify the evaluation of interaction effects between factors [30].

In the present study, a SPME method based on headspace SPME (HS-SPME) followed by gas chromatography-flame ionization detection (GC-FID) was used for the analysis of PAHs at microgram per liter levels in samples. The effects of several factors on the microextraction efficiency of analytes were studied based on a Box–Behnken design (BBD) [31].

In HS-SPME, the loaded fiber can be directly analyzed by GC, thus minimizing any potential analyte losses due to multistep processes. The prepared fiber exhibits many advantages over commercial SPME fibers, including high coating stability, a long service life, high adsorption capability, good selectivity for PAHs, a wide linear range, and low limits of detection (LODs), for the extraction of the studied PAHs, simple preparation, and cost effectiveness.

2. Experimental

2.1. Instruments

The analysis was performed with a gas chromatograph (model GC-17, Shimadzu, Japan) equipped with a GC-FID and a BP21 capillary column (25 m × 0.32 mm inner diameter, film thickness 0.5 μm). The GC conditions were as follows: the injector temperature was 280°C, and the detector temperature was 300°C. The column temperature was maintained at 80°C for 1 min then increased to 200°C at the rate of 10°C min⁻¹, and finally increased to 260°C at a rate of 20°C min⁻¹. Splitless injections were applied throughout. The high-purity nitrogen (99.999%) was applied as a carrier gas with the flow rate of 1 mL min⁻¹. Fourier transform infrared (FTIR) spectroscopy was carried out using a Nicolet Avatar 330 spectrometer. X-ray diffraction (XRD) measurements were performed on a D-Max 2200 VPC diffractometer (Japan) using Cu Kα radiation. Scanning electron microscopy (SEM) images were recorded on a JSM-6300 FSEM instrument (Japan). Thermogravimetric plots were obtained by a Netzsch-209 thermal gravimetric analyzer (Bavaria, Germany). Brunauer–Emmett–Teller (BET) analyses were carried out using an ASAP 2010 physisorption analyzer (Micromeritics Instrument Corporation, Norcross, USA). Samples were heat treated at 200°C under vacuum before measurement. An ultrasonic bath of type SONOREX DIGIPLUS DL 102 H (Bandelin electronic, Berlin, Germany) at 35 kHz of frequency and 120 W of power with power control from 20% to 100% was used for the preparation of GO dispersions.

2.2. Materials and reagents

Naphthalene (Naph), phenanthrene (Phen), anthracene (Anth), and chrysene (Chry), with the purity >99%, were supplied from Merck (Darmstadt, Germany). All organic solvents (chloroform, ethanol (EtOH), acetone, and acetonitrile) and

water with high-performance liquid chromatography grade were also purchased from Merck (Darmstadt, Germany). Graphite powder (99.95%) was purchased from Alfa Aesar (Tokyo, Japan). 1,3,5-Benzenetricarboxylic acid (H_3BTC) and 3-aminopropyltriethoxysilane (APTES) were purchased from Sigma–Aldrich (St. Louis, MO, USA). The stainless steel wire (316, 200 μm outer diameter) was obtained from an ironware factory. All real samples used for this study were filtered through a nylon 0.45 μm filter before use. Standard stock solutions containing 1,000 mg L^{-1} concentration of PAH compounds were prepared by dissolution of appropriate amount of each target analyte in methanol and then stored at 4°C prior to use.

2.3. Surface treatment of stainless steel fiber

The stainless steel fibers were cut into a length of 5.0 cm. The fibers were washed with acetone, methanol, and doubly distilled water, respectively, prior to use in order to remove the organic compounds. Subsequently, the cleaned wires were dried at room temperature. To oxidize the fiber surface, some oxidation solutions were trialed: hydrogen peroxide, sodium hydroxide, potassium dichromate, and sulfuric acid. The results demonstrated that the best compactness and coating uniformity were obtained only with sulfuric acid as oxidizing agent; therefore, the fibers were immersed in 0.1 mol L^{-1} solution of sulfuric acid for 120 min and then cleaned with pure water. Oxidation step was applied to bring $-\text{OH}$ groups to the surface of the stainless steel fibers and also to give chemical anchorage for the following reactions. Next, the fiber silylation was carried out by using various ratios of methanol and tetraethoxysilane. In this process, the fibers were immersed into a tetraethoxysilane-water-methanol (2:1:8, v/v) solution for 30 min and then dried in an oven at 150°C for 120 min. Finally, the fibers were rinsed 3 times with EtOH and dried with a stream of nitrogen.

2.4. Synthesis of GO

In this work, GO has been synthesized according to the method described in ref. [32]. Graphite powder (3.0 g) was added to the concentrated H_2SO_4 (70 mL, 98%) under agitation in an ice bath. Under vigorous shaking, $KMnO_4$ (9.0 g) was added slowly with the temperature of the suspension maintained lower than 20°C. The reaction pot was transferred to a 40°C oil bath and agitated vigorously for about 0.5 h. After this, 150 mL of water was added, and the solution was stirred at 95°C for 15 min. Then, 500 mL of water was added, and this was followed by the slow addition of H_2O_2 (15 mL, 30%), during which the color of the solution changed from dark brown to yellow-brown. Finally, the reaction mixture was filtered and washed with 1:10 HCl aqueous solution (250 mL) to remove metal ions. The solid product was then dried and diluted to 600 mL to make a graphite oxide aqueous suspension.

2.5. Fiber fabrication

The MOF-199/GO composite-coated fiber was prepared using a modified version of a previously reported method (Fig. 1) [33]. First, MOF-199 was prepared by adding H_3BTC (250 mg, 1.19 mmol) to dimethylformamide (DMF)/EtOH solution (40 mL, v/v, 1:1). $Cu(OAc)_2 \cdot H_2O$ (430 mg, 2.16 mmol)

was dissolved in water (20 mL). Then, GO (38.8 mg) that had been previously prepared was exfoliated for 30 min by ultrasonication in water (10 mL) to form a stable aqueous dispersion. The GO dispersion and $Cu(OAc)_2 \cdot H_2O$ solution were added sequentially to the H_3BTC solution with stirring. Triethylamine (250 μL) was then added to the mixture, which was agitated for 3 h. The solid product was collected and washed with DMF and finally dried. In the next step, to generate the silylated stainless steel fiber, the fiber was immersed into the APTES solution as a cross-linking agent for 12 h at room temperature, which mainly led to the formation of Si–O–Si bonds and amino-functionalized fiber. Then, the fibers were removed and immediately placed into an oven at 70°C to complete the silanization reaction. To coat the fiber with MOF-199/GO composites, the silylated fiber was inserted into a 0.2 wt.% aqueous composite dispersion for 2 h in a 70°C water bath. Then, it was removed and dried in air to give a thin layer of MOF-199/GO composites. Subsequently, it was transferred to an oven and heated at 70°C for 1 h. The coating process was repeated for 10 times. When the coating was prepared under the optimum conditions and coating on the stainless steel fiber was completed, the obtained thickness of coated composite was about 50 μm . Following this, the fibers were conditioned in the GC injection port under nitrogen gas at 280°C for 2 h and then used to extract target compounds.

2.6. Analytical procedures

The prepared MOF-199/GO composite-coated fiber was installed into a homemade SPME device. Prior to the SPME experiment, the fiber was conditioned at 260°C for 3 h under nitrogen to eliminate any transfer of impurities from the preparation process. Direct immersion of SPME is susceptible to contamination from the complex matrices in samples, leading to decrease in the life span, whereas HS-SPME can prevent the adsorption of other nonvolatile matrices and thus avoid damage to the fiber [34]. We adopted the HS extraction mode for the analytes. The HS extraction was conducted by placing the fiber into the extraction vial and suspending it above the sample solution. The sample volume and extraction space were kept consistent in every experiment. The microextraction step was performed under the optimum conditions, and the fiber was then withdrawn into the needle, removed from the microextraction vial, and then immediately inserted into the GC injection port at 280°C for thermal desorption. One background experiment of the fiber was performed after each extraction in order to eliminate or minimize the “carryover” effects. For HS-SPME, analyte sample solution (10.0 mL) was introduced to a 20.0 mL glass vial containing 2% (w/v) sodium chloride and then rapidly capped with a polytetrafluoroethylene-coated septum. A Teflon-coated stirring bar was applied to the agitated solution at 600 rpm, and the MOF-199/GO composite-coated fiber was exposed to the HS over the analyte sample solution at 65°C for 20 min for extraction. After extraction, the fiber was removed and immediately inserted into the GC inlet at 280°C for 4 min for analysis.

2.7. Sample preparation

Water samples were collected from the River Dez, Dezful, Iran; tap water and industrial wastewater samples were

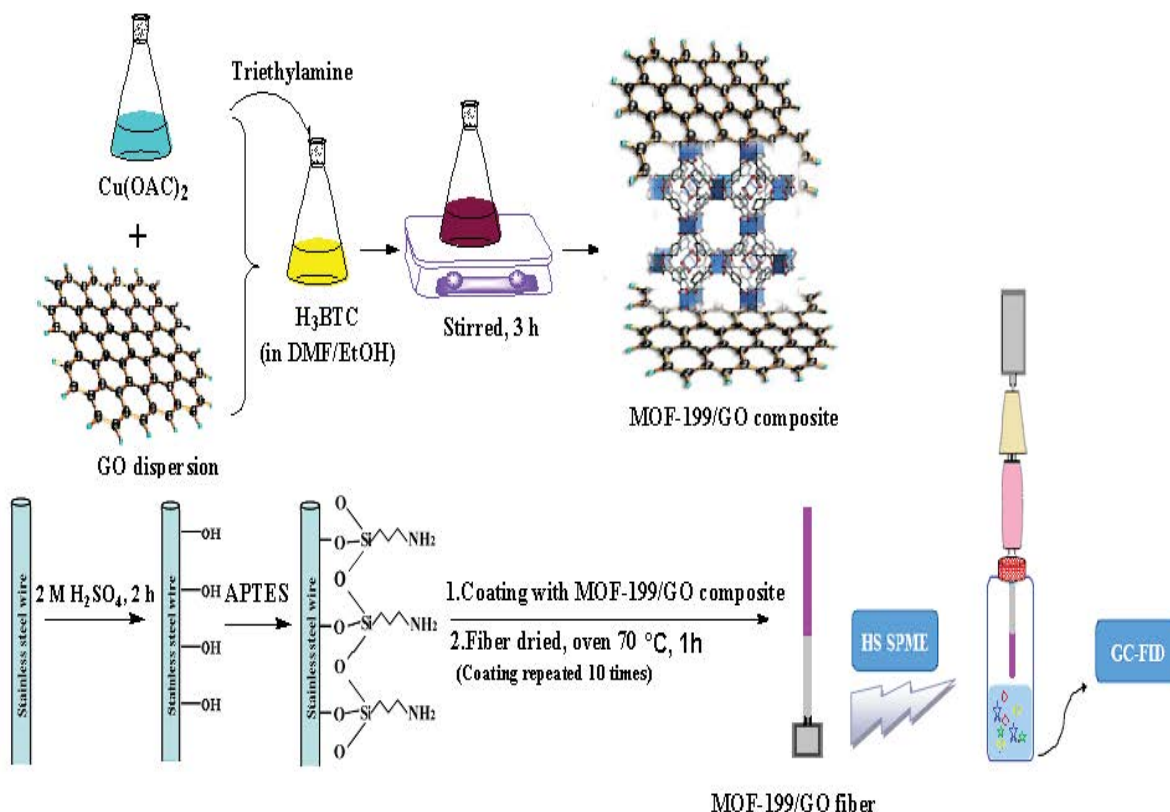


Fig. 1. Schematic fabrication process of MOF-199/GO composite-coated SPME fiber.

collected from our laboratory and petrochemical industry (Mahshahr, Iran), respectively. The samples were filtered through a Whatman No. 40 filter paper. Before analysis, 200 mL of sample was poured in a beaker and 2 mL of 1 mol L^{-1} HCl was added. The samples, while stirring, were heated for 15 min. The solution was filtered and diluted to 250 mL with distilled water after adjusting the pH to optimum value ($\text{pH} = 7$).

3. Results and discussion

3.1. Characterization of MOF-199/GO composite coatings

The FTIR spectra of synthesized GO, $\text{Cu}_3(\text{BTC})_2$ and $\text{Cu}_3(\text{BTC})_2/\text{GO}$ (MOF-199/GO) composite can be observed in Fig. S1. For GO, the characteristic features were the following: the absorption bands corresponding to the C=O group stretching at $1,737\text{ cm}^{-1}$, the C–OH stretching of the epoxide group at $1,050\text{ cm}^{-1}$, the O–H stretching vibrations of GO and the broad systemic adsorbed water peak at $3,428\text{ cm}^{-1}$. The absorption bands at $1,560\text{ cm}^{-1}$ can be ascribed to benzene rings. The sharp intense peak at $1,400\text{ cm}^{-1}$ can be related to carboxylic CO group.

The spectra of the composites and that of MOF-199 look rather alike. In the region of $700\text{--}1,300\text{ cm}^{-1}$, the bands at about $1,738$ and $1,442\text{ cm}^{-1}$ were assigned to the asymmetric stretching of carboxyl groups in H_3BDC , whereas the band at about $1,371\text{ cm}^{-1}$ was assigned to the symmetric stretching of carboxyl groups in H_3BDC [33,35]. The peak existed

at $1,442\text{ cm}^{-1}$ is dependent upon a combination of benzene ring stretching and deformation modes, and the peak around 700 cm^{-1} is related to the bending vibration of C–H benzene ring of H_3BDC . The FTIR absorption band observed at 507 cm^{-1} is assigned to a vibrational mode directly involving the Cu center. After GO incorporation, the characteristic GO peaks are swamped by the high-intensity $\text{Cu}_3(\text{BTC})_2$ peak owing to the rather small content of GO. Hence, the FTIR spectrum of $\text{Cu}_3(\text{BTC})_2/\text{GO}$ is similar to that of $\text{Cu}_3(\text{BTC})_2$. These results are in good accordance with the earlier reported data [33]. Fig. S2 shows the XRD patterns of the samples GO, $\text{Cu}_3(\text{BTC})_2$ and $\text{Cu}_3(\text{BTC})_2/\text{GO}$ composite. The XRD pattern of sample GO exhibited a strong peak at $2\theta = 11.6$, which can introduce an interlayer spacing of about 7.6 \AA indicating the presence of oxygen functionalities, which aided the hydration and exfoliation of GO layers in aqueous media. The XRD pattern of $\text{Cu}_3(\text{BTC})_2$ is in agreement with those found for well-defined $\text{Cu}_3(\text{BTC})_2$ crystals, indicating that the current material has the expected structure [33]. The XRD patterns of GO-incorporated $\text{Cu}_3(\text{BTC})_2$ showed the same diffraction patterns as of $\text{Cu}_3(\text{BTC})_2$, confirming that GO incorporation did not disturb or destroy the $\text{Cu}_3(\text{BTC})_2$ crystal structure. This phenomenon is attributed to the exfoliation/dispersion of GO in the polar solvents used during the material preparation [35,36].

SEM pictures of GO, $\text{Cu}_3(\text{BTC})_2$ and $\text{Cu}_3(\text{BTC})_2/\text{GO}$ composites are shown in Figs. 2(a)–(c). Fig. 2(a) displays the SEM image of the prepared GO that represents a layered and sheet-like structure with the large surface and

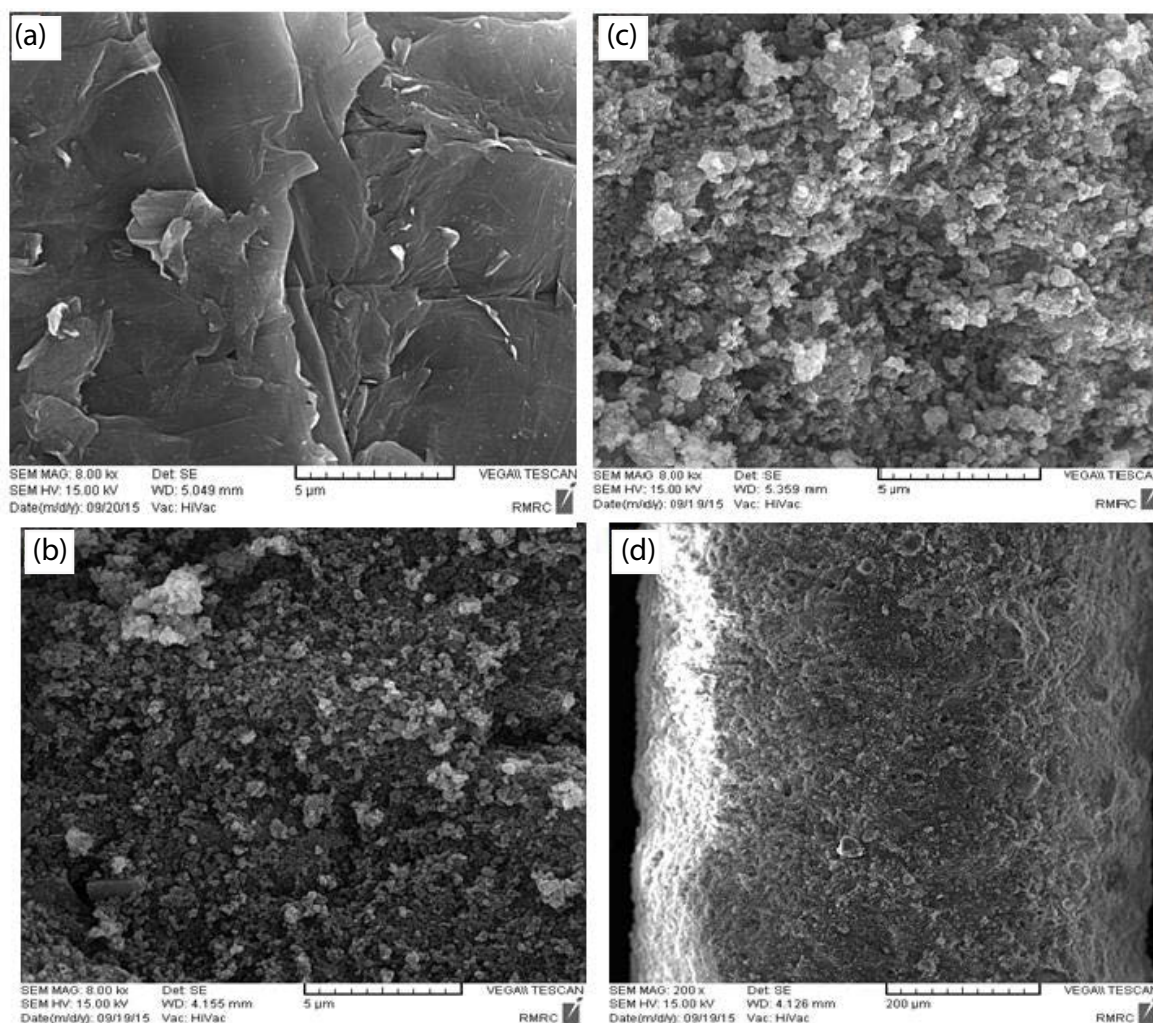


Fig. 2. Scanning electron micrographs of (a) GO, (b) Cu₃(BTC)₂ MOF, (c) Cu₃(BTC)₂/GO composites, (d) SPME fibers coated with Cu₃(BTC)₂/GO composite.

wrinkled edge. A comparison between Figs. 2(b) and (c) revealed that Cu₃(BTC)₂/GO composite showed uniform structure with more porosity than Cu₃(BTC)₂. SEM picture of fiber, after coating with Cu₃(BTC)₂/GO MOF composite, is presented in Fig. 2(d). The resulting pictures of fibers present highly cross-linked and porous morphological structure and indicates that the coating possessed a compact and homogeneous structure. However, in particular, the porous structure would be helpful for quick adsorption and desorption of target compounds for the microextraction in complex samples. The thermal stability of the prepared polymer was examined by TGA in the range 50°C–600°C at a heating rate of 10°C min⁻¹ and in a stream of nitrogen gas (Fig. S3). The results indicate that a mass loss occurred at about 300°C and the fastest mass loss occurred at 400°C. The weight loss of the polymer was quite small at temperatures below 300°C, but above this temperature, the weight loss was significant due to the decomposition of the composite. A surface area value of 204.56 m²g⁻¹ was determined by BET analysis for the synthesized MOF-199/GO hybrid composite fiber.

3.2. Optimization of conditions

In order to investigate and accomplish the work, the peak areas of the compounds under study were considered as the experimental response. Experiments were managed to optimize the chromatographic analysis of the analytes. Tests were then carried out to select the factors and the factor levels to be considered in the design of experiment (DOE) approach. In the development and application of the HS-SPME method, some conditions must be considered because of the different physicochemical properties of the compounds that will be extracted. Based on preliminary experiments carried out in our laboratory, at least 5 factors may affect the experimental response. These factors are extraction temperature (*T*), sample salt concentration (*SC*), sample pH, extraction time (*ET*), and stirring rate (*SR*). However, some of these parameters were not considered when designing the present experiments. In this extraction procedure, the effects of pH were investigated by a one-variable-at-a-time method. The sample pH was evaluated in the range of pH 3–12. The results indicated that the peak areas of the PAHs did not remarkably change in different pH

environments. This is perhaps owing to the fact that the PAHs were stable and not disassociated over a wide pH range because they had no ionizable groups [37]. In light of this, the sample pH was adjusted to be neutral in the experiments. The desorption time was evaluated at a temperature of 280°C in the range of 0.5–4 min. The results clearly indicated that increasing the desorption time up to 2 min enhances the extraction performance, and the maximum extraction efficiency of PAHs was achieved in 2 min and then remains approximately constant with longer ETs up to 4 min; therefore, 2 min was chosen as the optimum desorption time for HS-SPME of target analytes.

Other variables that are important in this microextraction were the effect of SC, *T*, and ET. It is obvious from the literature that increasing the ionic strength of solutions by adding salt is a more effective method of extracting analytes onto the solid phase of fiber because it minimizes the solubility of less polar compounds by forcing them to pass to the vapor phase (this is often termed ‘the salting out effect’) [38]. Therefore, SC could be a significant factor with an affirmative effect on extraction efficiency. Based on the results of the experiments, temperature values less than 30°C could not be maintained over a long period, and temperature values higher than 80°C could favor the loss of low molar mass PAHs. In addition, ET is another significant factor which can affect SPME extraction. Our results demonstrated that when the microextraction time was less than 5 min, the peak areas of the PAHs would decrease, while ETs of more than 60 min would lead to long analysis times. Therefore, according to the primary experiments, four process variables, namely, *T*, ET, SR, and SC, were considered for the next optimization step using the BBD approach to investigate their effect on the microextraction efficiency of PAHs by HS-SPME analysis.

3.2.1. Experimental design and optimization of HS-SPME by BBD

After performing some preliminary experiments, optimization of the microextraction conditions for the HS-SPME method was accomplished using a response surface design of BBD [39]. Response surface methodology was applied to optimize the extraction efficiency of PAHs on the MOF-199/GO composite-coated fiber and to investigate the correlation between response and factors. BBD was used to investigate the main effects, interaction effects, and quadratic effects of *T*, ET, SR, and SC. Extraction temperature (30°C–80°C), ET (5–25 min), SR (300–800 rpm), and SC (NaCl, 0%–25% w/v) are all variable input parameters, while a PAH concentration of 10 µg L⁻¹ was kept as a constant input parameter, and the peak areas for the compounds under study were considered as the experimental response. The four-factor three-level design was managed to get the second-order polynomial models using Minitab®16.2 statistical software. In case of four–three variables, a BBD is selected because it needs a fewer number of experiments than a central composite design. A design comprising 27 runs was developed, for which the nonlinear quadratic model can be expressed as Eq. (1):

$$Y = \beta_0 + \beta_1 X_1 + \beta_2 X_2 + \beta_3 X_3 + \beta_4 X_4 + \beta_{11} X_1^2 + \beta_{22} X_2^2 + \beta_{33} X_3^2 + \beta_{44} X_4^2 + \beta_{12} X_1 X_2 + \beta_{13} X_1 X_3 + \beta_{14} X_1 X_4 + \beta_{23} X_2 X_3 + \beta_{24} X_2 X_4 + \beta_{34} X_3 X_4 \quad (1)$$

where in this equation, *Y* is the estimated response, β_0 is a constant, β_1 , β_2 , β_3 , and β_4 are linear coefficients computed from the observed values of *Y* from experiments, and X_1 , X_2 , X_3 , and X_4 are independent variables. The terms ($X_1 X_2$, $X_1 X_3$, $X_1 X_4$, $X_2 X_3$, $X_2 X_4$, and $X_3 X_4$) and (X_1^2 , X_2^2 , X_3^2 , and X_4^2) represent the interaction and quadratic terms, respectively [18,19]. β_{12} , β_{13} , β_{23} , and β_{14} are interaction coefficients between the factors and β_{11} , β_{22} , β_{33} , and β_{44} are quadratic coefficients of β [39,40]. The *T*, ET, SR, and SC are the independent factors selected to investigate their influence on the microextraction efficiency. The number of runs (*N*) required to perform this design is defined as $N = 2k(k - 1) + C_0$ where *k* is the factor number and C_0 is the replicate number of the central point [38]. Thus, a total of 27 runs were performed to optimize these four variables in the current BBD.

For statistical calculations, the test factors were coded based on Eq. (2) [41]:

$$x_j = \frac{X_j - X_0}{\partial X} \quad (2)$$

where x_j is the coded value of the *j*th independent variable, X_j is the natural value of the *j*th independent variable, X_0 is the value of X_j at the center point, and ∂X presents the step change value. Thus, each independent variable was investigated at three different levels (low, medium, and high coded as -1, 0, and +1, respectively) as presented in Table 1.

The center point of this design was replicated three times and used to estimate the error. The values of the peak areas as response, *Y*, under the different experimental conditions are given in Table 2.

After fitting the obtained response variables using different models, the quadratic model was found to be the best-fitted model. In the equations for response, a positive value indicates a synergistic effect on the optimization, while a negative value demonstrates an antagonistic effect between the variables and the responses [42]. The results were analyzed based on the coefficient of determination (R^2), statistical residuals, and response surface plots.

3.2.2. Optimization of effective variables of HS-SPME by BBD

Twenty-seven experiments for the optimization were performed based on the BBD, and their responses are presented in Table 2. The main, interaction, and quadratic factor interactions were investigated in this design. To find the most essential

Table 1
The experimental variables and levels of the Box–Behnken design (BBD)

Factors	Abbreviation factors	Levels		
		Low (-1)	Central (0)	High (+1)
Temperature (°C)	<i>T</i> : X_1	30	55	80
Extraction time (min)	ET: X_2	5	15	25
Stirring rate (rpm)	SR: X_3	300	550	800
Salt concentration (% w/v)	SC: X_4	0	12.5	25

Table 2
The design matrix and the responses related to four analytes

Run no.	Variables				Responses			
	T (°C)	ET (min)	SR (rpm)	SC (% w/v)	PA1	PA2	PA3	PA4
1	0	0	–	+	75,289	103,584	93,288	98,849
2	–	0	–	0	41,295	62,386	54,606	60,586
3	–	–	0	0	44,340	66,532	46,132	64,222
4	–	+	0	0	88,443	122,860	97,197	114,842
5	0	0	+	–	106,716	147,942	123,984	129,233
6	–	0	+	0	45,883	68,533	49,737	66,582
7	+	0	–	0	39,295	61,580	41,936	58,622
8	+	+	0	0	109,322	145,534	12,173	133,172
9	0	–	–	0	40,995	51,136	31,563	48,221
10	0	0	–	–	50,205	73,602	59,792	71,513
11	+	0	0	+	91,743	128,162	110,821	105,332
12	0	0	0	0	106,073	150,890	122,975	141,123
13	0	–	+	0	79,963	114,391	93,936	98,838
14	0	0	0	0	116,659	141,922	133,156	132,213
15	+	0	+	0	107,862	156,274	124,992	139,963
16	0	0	0	0	106,099	152,858	122,945	141,242
17	0	–	0	+	75,125	93,947	87,732	79,672
18	–	0	0	+	68,934	89,597	78,724	76,942
19	+	–	0	0	48,623	78,542	68,034	67,592
20	0	+	0	+	102,271	149,953	122,384	135,983
21	0	+	–	0	195,737	136,541	105,272	119,967
22	+	0	0	–	55,623	83,542	107,380	81,986
23	0	+	0	–	98,567	138,468	107,892	122,163
24	0	0	+	+	88,286	119,946	107,892	108,761
25	–	0	0	–	45,936	69,767	51,793	63,594
26	0	+	+	0	122,271	174,731	142,869	159,533
27	0	–	0	–	46,642	76,757	65,939	69,534

PA1: Peak area (Chrysene), PA2: Peak area (Anthracene), PA3: Peak area (Naphthalene), PA4: Peak area (Phenanthrene).

effects and interactions, analysis of variance (ANOVA) was calculated using Minitab®16.2 statistical software. Tables 3–6 summarize the results obtained for the ANOVA study for all target compounds. A *p*-value of lower than 0.05 in the ANOVA table indicates the statistical significance of an effect at the 95% confidence level. An *F*-test was applied to evaluate the statistical significance of each term in the equation within a 95% confidence interval. However, according to this ANOVA and the results in Tables 3–6, the parameters (*T*: X_1), (*ET*: X_2), (*SC*: X_3), and (*SR*: X_4) had significant (*p* < 0.05) linear and positive outcome on the microextraction efficiency and peak area for the PAHs. The value of coefficients indicates that the effects of *ET* and *SR* factors on the responses were the most significant parameters. The response was also shown to be affected quadratically by the four factors (X_1^2 , X_2^2 , X_3^2 , and X_4^2). The interactions between *T* and *SR* (X_{14} : *T* × *SR*) and also *SC* and *SR* (X_{34} : *SC* × *SR*) for the extraction efficiency of all target PAHs are significant.

Therefore, the following response surface reduced quadratic equation was finally obtained for the surface area of target analytes:

$$\text{Peak area(Chrysene)} = 109,610 + 9,803X_1 + 23,410X_2 + 8,163X_3 + 17,347X_4 - 30,116X_1^2 - 9,491X_2^2 - 15,362X_3^2 - 16,804X_4^2 + 15,995X_1X_4 - 10,879X_3X_4$$

$$\text{Peak area(Phenanthrene)} = 148,557 + 14,497X_1 + 32,232X_2 + 7,926X_3 + 24,416X_4 - 37,378X_1^2 - 10,367X_2^2 - 19,633X_3^2 - 20,210X_4^2 + 22,137X_1X_4 - 14,494X_3X_4$$

$$\text{Peak area(Anthracene)} = 126,359 + 13,342X_1 + 25,245X_2 + 10,077X_3 + 21,438X_4 - 34,441X_1^2 - 12,725X_2^2 - 13,830X_3^2 - 20,230X_4^2 + 21,906X_1X_4 - 12,397X_3X_4$$

$$\text{Peak area(Naphthalene)} = 138,193 + 11,658X_1 + 29,798X_2 + 5,626X_3 + 20,429X_4 - 34,738X_1^2 - 12,200X_2^2 - 20,972X_3^2 - 18,834X_4^2 - 18,836X_1X_4 - 11,952X_3X_4$$

Table 3
ANOVA and model statistical summary and quality of the quadratic model for the microextraction and determination of Chrysene

Source	DF ^a	Sum of square	Mean squares	F	P
Regression	14	19,196,094,522	1,371,149,609	18.48	0.000
Linear	4	12,140,402,384	611,635,544	8.25	0.002
T	1	1,153,205,314	1,661,517,647	22.40	0.000
ET	1	6,576,477,661	700,888,022	9.45	0.010
SC	1	799,663,807	1,103,627,981	14.88	0.002
SR	1	3,611,055,602	894,727,500	12.06	0.005
Square	4	5,254,942,655	1,313,735,664	17.71	0.000
T × T	1	3,163,893,643	4,837,312,230	65.21	0.000
ET × ET	1	13,454,840	480,459,730	6.48	0.026
SC × SC	1	571,574,880	1,258,557,454	16.97	0.001
SR × SR	1	1,506,019,291	1,506,019,291	20.30	0.001
Interaction	6	1,800,749,484	300,124,914	4.05	0.019
T × ET	1	68,856,804	68,856,804	0.93	0.354
T × SC	1	43,046,721	43,046,721	0.58	0.461
T × SR	1	1,023,328,110	1,023,328,110	13.80	0.003
ET × SC	1	153,499,710	153,499,710	2.07	0.176
ET × SR	1	38,651,089	38,651,089	0.52	0.484
SC × SR	1	473,367,049	473,367,049	6.38	0.027
Residual error	12	890,151,618	74,179,302		
Lack-of-fit	10	815,625,728	81,562,573	2.19	0.354
Pure error	2	74,525,891	37,262,945		
Total	26	20,086,246,140			

a: Degree of freedom.

Table 4
ANOVA and model statistical summary and quality of the quadratic model for the microextraction and determination of Anthracene

Source	DF ^a	Sum of square	Mean squares	F	P
3	14	34,202,467,528	2,443,033,395	24.05	0.000
Linear	4	22,895,843,306	863,772,741	8.50	0.002
T	1	2,521,811,140	2,513,054,127	24.74	0.000
ET	1	12,466,692,960	1,189,502,784	11.71	0.005
SC	1	753,841,860	1,197,018,466	11.79	0.005
SR	1	7,153,497,345	1,366,554,640	13.46	0.003
Square	4	8,158,852,738	2039,713,184	20.08	0.000
T × T	1	4,981,512,178	7,451,080,033	73.37	0.000
ET × ET	1	1,056,738	573,212,164	5.64	0.035
SC × SC	1	997,834,448	2,055,705,987	20.24	0.001
SR × SR	1	2,178,449,374	2,178,449,374	21.45	0.001
Interaction	6	3,147,771,485	524,628,581	5.17	0.008
T × ET	1	28,430,224	28,430,224	0.28	0.606
T × SC	1	153,636,025	153,636,025	1.51	0.242
T × SR	1	1,960,142,802	1,960,142,802	19.30	0.001
ET × SC	1	8,136,756	8,136,756	0.08	0.782
ET × SR	1	157,063,556	157,063,556	1.55	0.237
SC × SR	1	840,362,121	840,362,121	8.27	0.014
Residual error	12	1,218,730,120	101,560,843		
Lack-of-fit	10	1,150,765,406	115,076,541	3.39	0.249
Pure error	2	67,964,715	33,982,357		
Total	26	35,421,197,649			

a: Degree of freedom.

Table 5
ANOVA and model statistical summary and quality of the quadratic model for the microextraction and determination of Naphthalene

Source	DF ^a	Sum of square	Mean squares	F	P
Regression	14	26,050,838,454	1,860,774,175	22.00	0.000
Linear	4	16,517,001,790	786,901,098	9.30	0.001
T	1	2,136,107,568	2,214,231,295	26.18	0.000
ET	1	7,647,518,341	1,356,006,194	16.03	0.002
SC	1	1,218,450,380	958,769,015	11.34	0.006
SR	1	5,514,925,501	1,228,489,402	14.53	0.002
Square	4	6,792,176,231	1,698,044,058	20.08	0.000
T × T	1	4,194,780,598	6,326,352,487	74.80	0.000
ET × ET	1	113,414,033	863,552,434	10.21	0.008
SC × SC	1	301,353,414	1,020,137,680	12.06	0.005
SR × SR	1	2,182,628,187	2,182,628,187	25.81	0.000
Interaction	6	2,741,660,433	456,943,405	5.40	0.006
T × ET	1	1,078,482	1,078,482	0.01	0.912
T × SC	1	41,319,184	41,319,184	0.49	0.498
T × SR	1	1,919,535,156	1,919,535,156	22.70	0.000
ET × SC	1	11,522,630	11,522,630	0.14	0.718
ET × SR	1	153,462,544	153,462,544	1.01	0.203
SC × SR	1	614,742,436	614,742,436	7.27	0.019
Residual error	12	1,014,879,966	84,573,330		
Lack-of-fit	10	945,580,732	94,558,073	2.73	0.298
Pure Error	2	69,299,234	34,649,617		
Total	26	27,065,718,420			

a: Degree of freedom.

Table 6
ANOVA and model statistical summary and quality of the quadratic model for the microextraction and determination of Phenanthrene

Source	DF ^a	Sum of square	Mean squares	F	P
Regression	14	26,948,118,836	1,924,865,631	28.33	0.000
Linear	4	3,079,721,856	769,930,464	11.33	0.000
T	1	2,303,902,624	2,303,902,624	33.91	0.000
ET	1	903,070,114	903,070,114	13.29	0.003
SC	1	1,175,890,296	1,175,890,296	17.31	0.002
SR	1	1,059,455,225	1,059,455,225	15.59	0.000
Square	4	7,168,154,938	1,792,038,734	26.38	0.000
T × T	1	6,435,839,784	6,435,839,784	94.73	0.005
ET × ET	1	793,797,067	793,797,067	11.68	0.000
SC × SC	1	2,345,732,181	2,345,732,181	34.53	0.000
SR × SR	1	1,891,787,408	1,891,787,408	27.84	0.008
Interaction	6	2,105,479,305	350,913,217	5.16	0.006
T × ET	1	55,950,400	55,950,400	0.82	0.382
T × SC	1	24,990,001	24,990,001	0.37	0.555
T × SR	1	1,419,217,256	1,419,217,256	20.89	0.001
ET × SC	1	3,389,281	3,389,281	0.05	0.827
ET × SR	1	30,531,150	30,531,150	0.45	0.515
SC × SR	1	571,401,216	571,401,216	8.41	0.013
Residual error	12	815,293,556	67,941,130		
Lack-of-fit	10	761,651,856	76,165,186	2.84	0.288
Pure error	2	53,641,701	26,820,850		
Total	26				

a: Degree of freedom.

The statistical significance of the quadratic model was predicted by ANOVA based on PA1–PA4, peak areas of Chry, Naph, Phen, and Anth, respectively, as the responses (Table 2). The result revealed that the F -value of the fitted models for the Chry, Naph, Phen, and Anth peak areas were 18.48, 24.02, 22.00, and 28.33, respectively. A p -value less than 0.05 proved the ability and suitability of the model for good and practical prediction of the behavior of all analytes during the microextraction process. The lack of fit test, which determines the failure of the fitted model to represent experimental data in the experimental domain at points not used in the regression equation [43], was applied. The lack of fit F -values of model for the simultaneous microextraction of Chry, Naph, Phen, and Anth were 2.19, 3.39, 2.73, and 2.84, respectively. The “lack of fit F -value” responses pointed out that the F -values are not significant relative to the pure error. The p -values for the “lack of fit” test for Chry, Naph, Phen, and Anth were 0.354, 0.249, 0.298, and 0.288, respectively; thus, a nonsignificant “lack of fit” is good, and the regression model was strongly significant.

The values of the R^2 (0.956, 0.966, 0.9706, and 0.957) and the adjusted R^2 (0.910, 0.920, 0.936, and 0.910) for the simultaneous microextraction of all target PAHs indicated very good agreement between the experimental data and the predicted values of responses and demonstrated that the response surface quadratic model is the most adequate for predicting the efficiency of simultaneous microextraction of Chry, Naph, Phen, and Anth onto the MOF-199/GO composite-coated fibers. This means that the calculated models could explain more than 90% of the results (or of the variability of the response).

The results indicated that the model applied to fit the response variables was significant and appropriate to represent the relation between the response and the independent variables. Another convenient expression of this model is demonstrated using the actual and model predicted data. Fig. 3 shows the plot of the predicted values versus actual values to check the capability of the models to fit the simultaneous microextraction of analytes. The good fitting corresponds to the plots of experimental peak area versus calculated values, which shows the high potency of the model for prediction of the behavior of the system.

3.2.3. Effects of interactive variables

The best way to represent the influence of the independent variables on the dependent variables is to draw response

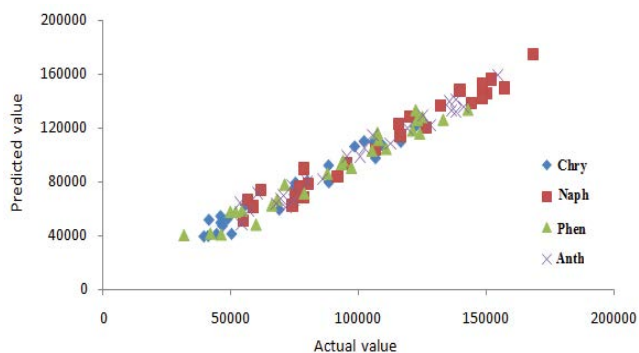


Fig. 3. Predicted vs. actual data for the analytes under the experimental conditions.

surface curves for the model, which were done by varying two variables through the experimental range and keeping the other two constant at the central point.

In this study, to evaluate the interactive effect of each pair of variables on the PAH microextraction and response, the use of three-dimensional (3D) graphs of the model is suggested. The interactions between the three significant variables and the relationship between four responses and experimental levels for different variables were demonstrated by the 3D plots in Figs. 4(a) and (b). The combined effects of the SC and SR on the peak area of all analytes, with other factors fixed at their center points, are shown in these Figs. 4(a)–(c) in which the curvature indicates a strong interaction between these two factors. The maximum response was reached when the SR was close to 550 rpm and the SC was slightly higher than 12.5% (w/v). However, the saturation problems appeared when the SC was higher, and the higher values of SC were observed to show a negative effect on the response.

Figs. 4(a), (b), and (d) represent the interaction of T and SR on the peak areas of all analytes. The microextraction efficiency and peak area increase with rising temperature, and the maximum peak areas of analytes were achieved at the T of $\sim 55^\circ\text{C}$ and an SR of ~ 550 rpm. It was also found that at more than 55°C , a significant decrease in the peak area was observed. This is most probably due to a decrease in the partition coefficient of analytes between the HS phase and the fiber because adsorption process is an equilibrium phenomena [18]. However, higher temperatures are not practical since the target analytes do not remain adsorbed onto the fiber and tend to be desorbed to the HS. Fig. 4(b) also reveals the remarkable contribution of the SR to increasing mass transfer that makes possible the rapid uptake and fast establishment of equilibrium. As can be seen in Fig. 4(b), parallel with the increase in the SR, the peak area of the corresponding compound increased, and the maximum response for all analytes was achieved at an SR of ~ 550 to 600. This may be because of the fact that an increase in the stirrer speed of the sample solution raises the mass transfer in the aqueous phase, which enhances convection in the HS, and accordingly, the microextraction efficiency between the aqueous phase and HS can be obtained more rapidly. Namely, sample agitation reduces the time required to reach the equilibrium by increasing the diffusion of the analytes toward the fiber. Indeed, this parameter was one of the most positive significant factors on the extraction [44,45].

The optimization plot (Fig. 5) demonstrates the predicted conditions for the optimum point and the desirability of the prediction. Each individual plot in the figure shows the way each factor influences the response (peak area). According to the whole results of the optimization study, the following experimental conditions were selected: T , 55°C ; ET, 15 min; SR, 550 rpm; and SC (NaCl, w/v, %), 12.5%.

3.2.4. Optimization of BBD by desirability function for the preconcentration of analytes

The next step was to find the optimum condition of each factor to obtain the maximum response. The desirability profile for predicted values was achieved using the Minitab[®]16.2 statistical software for the optimization of the process and to optimize variables including T , ET, SC, and SR. The minimum,

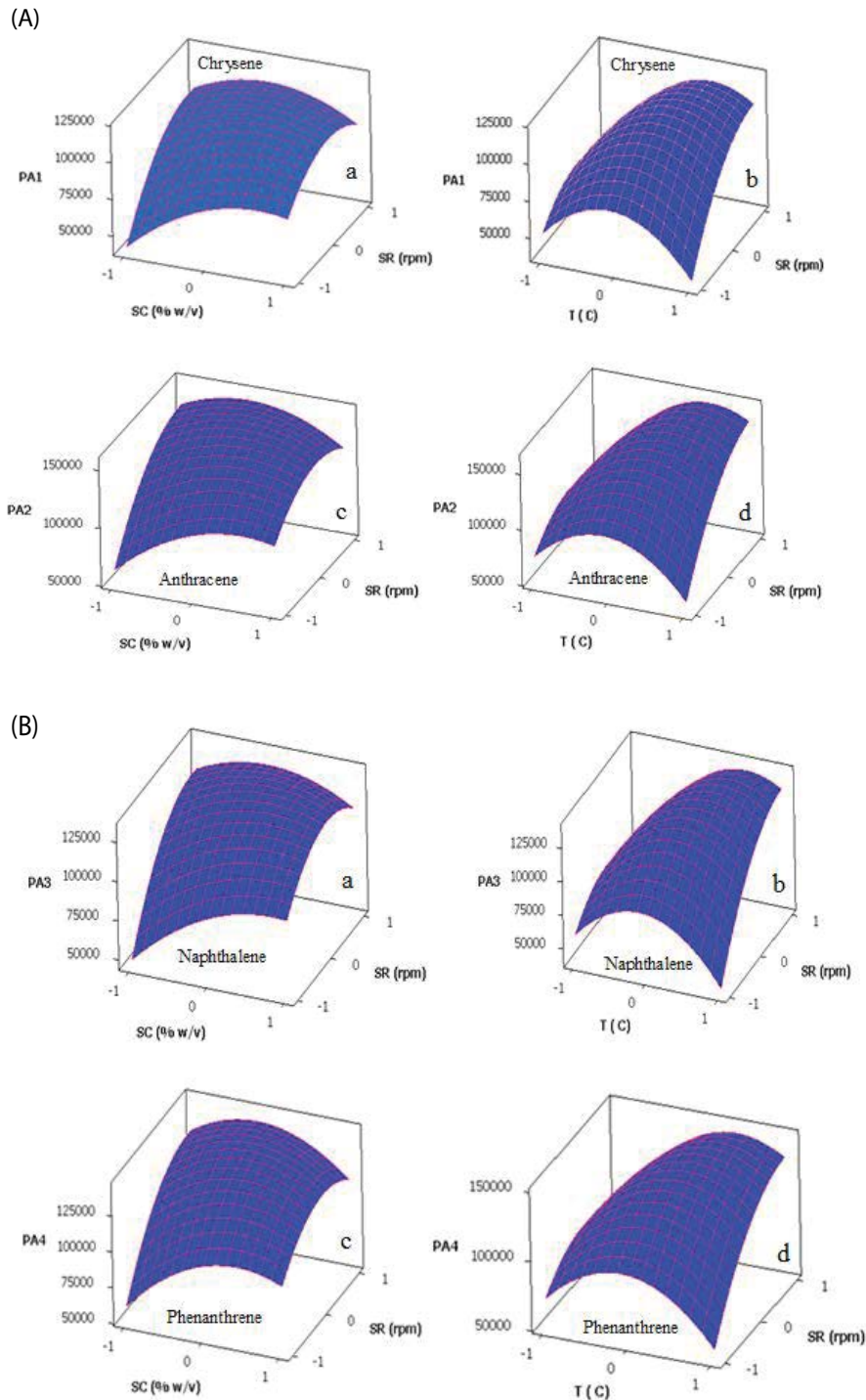


Fig. 4. (A) Response surface graphs for the 24 BBD: Effect of interaction between extraction salt concentration-stirring rate and temperature-stirring rate (a and b) for Chrysene and (c and d) for Anthracene, (B) Response surfaces for the 24 BBD: Effect of interaction between extraction salt concentration-stirring rate and temperature-stirring rate (a and b) for Naphthalene and (c and d) for Phenanthrene.

middle, and maximum values of desirability were configured as 0.0, 0.5, and 1.0, respectively. A desirability value close to 1 indicates the most desired conditions and the corresponding responses.

Optimum values of 60.8°C, 25 min, 694 rpm and 12.5% (w/v) were obtained for the T, ET, SR, and SC, respectively, with a composite desirability of 0.9674 (Fig. 5). As a general result, it was realized that the low molecular weight PAHs

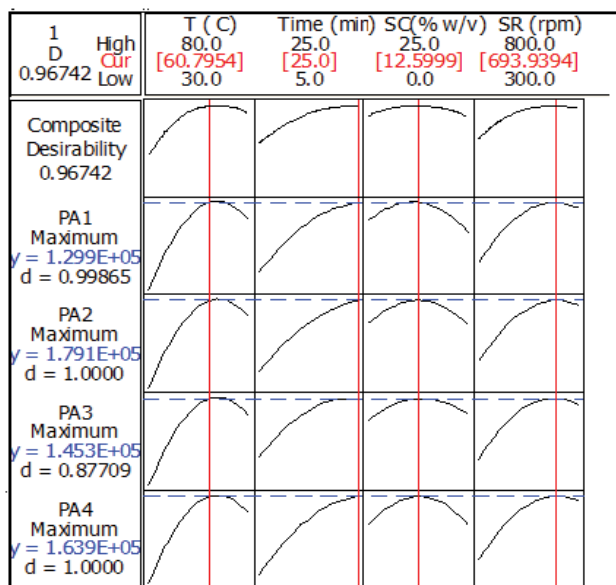


Fig. 5. Profiles for predicted values and desirability function for the four analytes under the experimental conditions. The vertical red line indicated current values after optimization.

represented single desirability values lower than those obtained for the other compounds; this behavior could be explained by considering the higher volatility of these analytes, thus requiring different extraction conditions than those applied for the other compounds [46]. After optimization of the process, some experiments were performed at the optimum conditions from which the reliability of the model prediction was approved. The results were in good accordance with the predicted values.

3.3. Method validation

To assess the proposed method, the linearity, matrix effect, sensitivity, recovery, precision, and stability were investigated under the optimum conditions for two types of industrial wastewater, river water, mineral water, and tap water using an MOF-199/GO composite-coated fiber. Figures of merit for this method, including dynamic linear ranges, correlation coefficients, relative standard deviations (RSD), LODs, and enrichment factors (EFs), are presented

in Table 7. Calibration curves were plotted using aqueous solutions spiked with a series of PAHs of different concentrations. Calibration curves (average of five injections and based on peak areas) were obtained over the concentration range of interest ($0.1\text{--}200\ \mu\text{g L}^{-1}$) for all compounds. Calibration curve correlation coefficients were higher than 0.997 in all cases.

The LODs and limits of quantification (LOQs) were defined as a response equivalent to three times or ten times the average height of the blank baseline noise, respectively, and were obtained by analyzing the PAH mixture at the lowest sample concentration divided by the slope of the calibration curves. LODs ranged from $0.027\text{--}0.041\ \mu\text{g L}^{-1}$. The good detectability obtained in this range is appropriate for all targets proposed in this work. The LOQ values were calculated for ten replicate runs in the range of $0.09\text{--}0.136\ \mu\text{g L}^{-1}$.

The EFs, defined as the ratio of PAH concentrations after extraction and that before extraction, were in the range from 163.6 to 193.7.

In order to find the extraction recovery and the accuracy of this method, standard addition tests were applied. The extraction recoveries (R) of PAHs were calculated from Eq. (3) [47]:

$$R(\%) = \frac{(C_{\text{found}} - C_{\text{real}})}{C_{\text{added}}} \times 100 \quad (3)$$

where C_{found} , C_{real} , and C_{added} are the concentrations of PAHs after spike of a known amount of standard in the real samples, the actual amount of PAHs in the real sample, and the concentration of the known amount of standard that has been added to the real sample, respectively. As shown in Table 8, the recoveries were in the range of 93%–103.0%. This approach performed well in the environmental samples and showed satisfactory recovery, implying that it can perform well in samples with an environmental matrix. The above results confirmed a small influence of the matrix composition on the extraction process.

A precision study, characterized in terms of %RSD for intraday precision (repeatability) and interday precision (reproducibility), was made by analyzing industrial wastewater, river water, mineral water, and tap water at three concentration levels on the same day ($n = 5$) and then for 5 days for all samples. The precision results of the analysis were acceptable, and low RSD values were obtained; single-fiber repeatability for five replicate analyses at the spiking level

Table 7
Quantitative results from extraction of polycyclic aromatic hydrocarbons (PAHs)

Analyte	L.R ($\mu\text{g L}^{-1}$)	LOD ($\mu\text{g L}^{-1}$)	LOQ ($\mu\text{g L}^{-1}$)	EF	RSD ^a (%)Interday	RSD ^a (%)Intraday
Chrysene	0.1–200	0.027	0.090	168.6	1.60	2.30
Phenanthrene	0.1–200	0.031	0.110	193.7	1.77	2.23
Anthracene	0.1–200	0.040	0.124	188.5	2.13	2.3
Naphthalene	0.1–200	0.041	0.136	163.6	1.73	2.10

L.R: Linear range.

LOD: Limit of detection.

LOQ: Limit of quantification.

EF: Enrichment factor, defined as the ratio of PAH concentrations after extraction and that before extraction.

a: Concentration of PAHs = $5\ \mu\text{g L}^{-1}$

Table 8
Results from recovery of polycyclic aromatic hydrocarbons (PAHs) in industrial wastewater, river water, tap water, and drinking water samples ($n = 5$)

Sample	Analyte	Original contents Found (μgL^{-1})	Recovery spiked sample (found) ^a		
			1 (μgL^{-1})	50 (μgL^{-1})	150 (μgL^{-1})
Industrial wastewater (1)	Chry	ND ^b	99.0 (0.99)	95.4 (47.70)	97.3 (145.95)
	Phen	0.34	96.0 (1.30)	97.0 (48.84)	95.8 (144.04)
	Anth	0.65	98.0 (1.63)	98.5 (49.90)	98.5 (148.35)
	Naph	0.45	96.0(1.41)	97.8 (49.35)	99.4 (149.55)
Industrial wastewater (2)	Chry	ND	100.0 (1.00)	98.2 (49.10)	95.6 (143.40)
	Phen	0.48	95.0 (1.43)	98.5 (50.21)	99.5 (149.73)
	Anth	0.66	100.0 (1.66)	101.5 (51.41)	101.0 (152.16)
	Naph	1.07	102.0 (2.09)	93.8 (47.97)	97.7 (147.62)
Industrial wastewater (3)	Chry	ND	101.3 (1.01)	98.2 (49.10)	103.0 (154.50)
	Phen	1.18	98.0 (2.16)	100.1 (51.23)	99.1 (149.83)
	Anth	0.84	100.0 (1.84)	98.7 (50.19)	100.1 (150.99)
	Naph	ND	99.0 (0.99)	101.2 (50.60)	99.1 (148.65)
River water	Chry	ND	96.0 (0.96)	98.7 (49.35)	99.3 (148.95)
	Phen	ND	100.0 (1.00)	102.0 (51.00)	99.7 (49.85)
	Anth	ND	95.0 (0.95)	99.8 (49.90)	98.4 (147.60)
	Naph	ND	97.0 (0.97)	97.1 (48.55)	101.2 (151.80)
Tap water	Chry	ND	93.0 (0.93)	98.6 (49.30)	100.3 (150.45)
	Phen	ND	93.0 (0.93)	103.0 (51.50)	97.7 (146.55)
	Anth	ND	96.0 (0.96)	99.2 (49.60)	97.5 (146.25)
	Naph	ND	99.0 (0.99)	98.0 (49.00)	98.5 (147.75)
Drinking water	Chry	ND	97.0 (0.97)	100.3 (50.15)	99.2 (148.80)
	Phen	ND	99.0 (0.99)	101.0 (50.50)	96.7 (145.05)
	Anth	ND	97.0 (0.97)	97.5 (48.75)	100.4 (150.60)
	Naph	ND	99.0 (0.99)	98.5 (49.25)	102.2 (153.30)

a: Relative standard deviations for all measurements for five replicates were less than 3%.

b: ND: Not detected.

of $5 \mu\text{g L}^{-1}$ of each target analyte varied from 1.60%–2.13% and from 2.10%–2.30% (Table 7) for the intraday and interday HS-SPME-GC-FID methods, respectively. The fiber-to-fiber reproducibility evaluated using three fibers ranged from 5.2% to 12.8% under the same conditions.

3.4. Assay of real samples

Some PAHs are recognized as potential carcinogens and show tumorigenic activity and endocrine-disrupting activity in mammals [48]. Generally, their concentration levels are very low in different real water samples, and thereby, pre-concentration is usually necessary before they can be efficiently determined. Therefore, this method was employed for pre-concentration and determination of target analytes in different water and wastewater samples. The results of analyses ($n = 5$) are presented in Table 8 for real samples spiked with 1, 50, and $150 \mu\text{g L}^{-1}$ levels of target analytes. Some of the compounds included in this study were found at trace levels in the water samples, and their concentration was evaluated using the proposed method. Recovery studies of real samples were performed by five different spiked real

samples; as it is obvious from Table 8, the recoveries were between 93.03% and 103% in all cases, and the RSD values were lower than 3%. These recoveries demonstrated that the complex real sample matrix had insignificant effects on the extraction efficiency of the MOF-199/GO fiber. The quantitative analysis of PAHs in a low concentration even in a complex waste and wastewater and natural water sample showed that the proposed method can meet the conditions of trace analysis of mentioned PAHs in complex real matrices. In addition, convenient operation, simple setup, low cost, and good sensitivity are further advantages of the proposed method. Fig. 6 shows the typical chromatograms of analytes in standard solution ($10 \mu\text{gL}^{-1}$ of each PAHs) and unspiked and spiked real samples. The results indicate that there are no additional or interfering peaks in the chromatograms of the real samples, thus demonstrating the performance of this method as a clean-up technique.

3.5. Comparison of this adsorbent and method with other methods

Table 9 compares the results of the proposed method with those of other reported fiber coating, such as monolithic

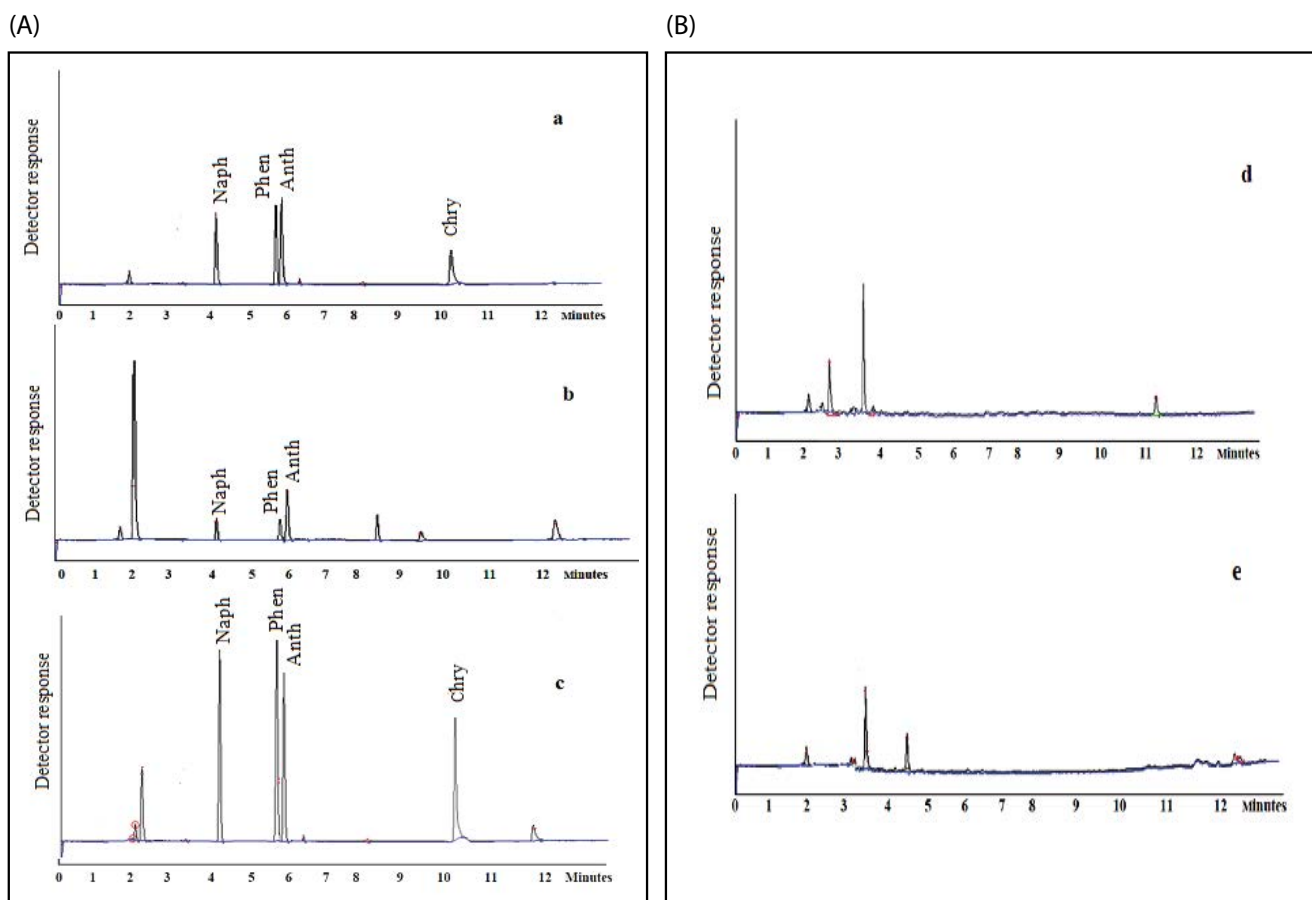


Fig. 6. (A) Chromatograms of (a) standard solution of chrysene, anthracene, naphthalene, and phenanthrene ($10 \mu\text{gL}^{-1}$ of each PAHs); (b) unspiked industrial wastewater (1) (c) spiked industrial wastewater (1) (spiked with 50 ng L^{-1}); (e) river water after extraction using MOF-199/GO composite-coated SPME fiber. Conditions: extraction temperature: 55°C ; extraction time: 15 min; stirring rate: 550 rpm; salt concentration: 12.5%. (B) Chromatograms of unspiked (d) river water and (e) drinking water after extraction using MOF-199/GO composite-coated SPME fiber. Conditions: extraction temperature: 55°C ; extraction time: 15 min; stirring rate: 550 rpm; salt concentration: 12.5%.

Table 9

Comparative study of performance method with previously reported methods for determination of PAHs in different water samples

Fiber type	Linear range (μgL^{-1})	LOD (μgL^{-1})	R (%)	RSD (%)	Ref.
Sol- gel ENPF ^a	0.5–10	0.05–0.16	83–108	≤ 8	[2]
PANI ^b	0.02–10 pgmL^{-1}	0.1–6	82–111	8.80–16.8	[10]
PDMS/MOF-199 ^c	0.01–2.0	0.004	78–110.3	9.3	[13]
TiO ₂ NS-Ti ^d	0.05–300	0.008–0.043	86.2–112	≤ 5.23	[48]
Monolithic-GRF ^e	0.05–200	0.004–0.05	79–116	9.3	[49]
GO/fused silica ^f	0.05–200	0.08	84–118.2	≤ 5	[50]
Copper fiber ^g	0.05–100	0.001–0.01	86.2–115	0.6–3.6	[51]
Yb–MOF coating ^h	10–1000 ng L^{-1}	0.07–1.67 ng L^{-1}	69.8–114.4	≤ 10	[52]
MWCNTs-HF ⁱ	0.02–100	0.009–0.013	–	≤ 3	[53]
MOF-199/GO ^k	0.1–200	0.027–0.041	93–103	≤ 3	This work

a: Sol-gel ethoxylated nonylphenol fiber; b: Polyaniline-based fiber; c: Polydimethyl siloxane/metal-organic-framework-coated fiber; d: Titanium dioxide nanosheet coating on a titanium wire; e: Monolithic graphene fiber; f: Graphene oxide/fused silica; g: Copper fiber-in-tube SPME; h: Porous ytterbium-based metal-organic framework (Yb–MOF) coating; i: Multiwalled carbon-nanotube-loaded hollow fiber; k: Metal-organic framework-199@graphene oxide fiber.

graphene, PDMS/MOF-199, GO/fused silica, titanium dioxide nanosheet coating, and MWCNTs. The abovementioned method exhibits very low LOD values for target analytes. These data clearly indicate that the established HS-SPME-GC-FID procedure with MOF-199/GO fiber is simple, rapid, environment friendly, and reliable for selective preconcentration and sensitive analysis of target compounds in industrial waste and real natural water samples. Also, it can be seen from the results that the analytical figures of merit for our proposed method are comparable or better than those previously reported (Table 9). This method gives comparable analytical results to previously reported techniques and can present good quantification extraction efficiency, a wide linear range, and better reproducibility with respect to the other techniques.

In addition, the method based on MOF-199/GO composite-coated fiber HS-SPME-GC-FID detection has advantages over some previously reported methods of no solvent consumption, reduced operation procedure, and no requirement to add further purification procedure for removing co-extractant; this method brings the possibility to obtain analysis of target compounds in the presence of known and/or unknown interferences in different complex matrices.

4. Conclusions

In the present study, a new SPME fiber coating based on MOF-199/GO hybrid nanocomposite was fabricated. Statistical DOE was successfully utilized for the optimization of this method for the determination of four PAH compounds in different industrial wastewater and natural water samples, using HS-SPME. The advantage of HS-SPME was combined with GC-FID to minimize matrix interferences and provide a selective procedure for trace analysis of Chry, Naph, Phen, and Anth in different wastewater and water samples. Good average percentage recoveries and repeatability in spiked samples were obtained for all studied compounds.

In the present work, silica fiber was displaced with stainless steel wire with the characteristics of good mechanical properties and easy acquirement, flexible, and nonfragile. By selection of stainless steel as a substrate material of SPME fibers and using MOF-199/GO nanocomposites as a coating material, the mechanical stability and extraction performances were improved. No significant change was observed in the extraction performance of the proposed SPME fiber over at least 20 extractions.

Acknowledgement

The authors greatly appreciate the financial support of this work by the Research Council of Shahid Chamran University of Ahvaz, Iran.

References

- [1] G. Purcaro, M. Picardo, L. Barp, S. Moret, L.S. Conte, Direct-immersion solid-phase microextraction coupled to fast gas chromatography mass spectrometry as a purification step for polycyclic aromatic hydrocarbons determination in olive oil, *J. Chromatogr. A*, 1307 (2013) 166–171.
- [2] A. Es-haghi, V. Hosseinasab, H. Bagheri, Preparation, characterization and applications of a novel solid-phase microextraction fiber by sol-gel technology on the surface of stainless steel wire for determination of poly cyclic aromatic hydrocarbons in aquatic environmental samples, *Anal. Chim. Acta*, 813 (2014) 48–55.
- [3] B. Delgado, V. Pino, J.H. Ayala, V. González, A.M. Afonso, Nonionic surfactant mixtures: a new cloud-point extraction approach for the determination of PAHs in seawater using HPLC with fluorimetric detection, *Anal. Chim. Acta*, 518 (2004) 165–172.
- [4] L. Xie, S. Liu, Z. Han, R. Jiang, H. Liu, F. Zhu, F. Zeng, C. Su, G. Ouyang, Preparation and characterization of metal-organic framework MIL-101(Cr)-coated solid-phase microextraction fiber, *Anal. Chim. Acta*, 853 (2015) 303–310.
- [5] M. Engraff, C. Solere, K.E.C. Smith, P. Mayer, I. Dahllöf, Aquatic toxicity of PAHs and PAH mixtures at saturation to benthic amphipods: linking toxic effects to chemical activity, *Aquat. Toxicol.*, 102 (2011) 142–149.
- [6] A. Mehdinia, E. Khojasteh, T.B. Kayyal, A. Jabbari, Magnetic solid phase extraction using gold immobilized magnetic mesoporous silica nanoparticles coupled with dispersive liquid-liquid microextraction for determination of polycyclic aromatic hydrocarbons, *J. Chromatogr. A*, 1364 (2014) 20–27.
- [7] W.D. Wang, Y.M. Huang, W.Q. Shu, J. Cao, Multiwalled carbon nanotubes as adsorbents of solid-phase extraction for determination of polycyclic aromatic hydrocarbons in environmental waters coupled with high-performance liquid chromatography, *J. Chromatogr. A*, 1173 (2007) 27–36.
- [8] Z. Li, L.C. Romanoff, D.A. Trinidad, N. Hussain, R.S. Jones, E.N. Porter, D.G. Pat-terson, A. Sjödin, Measurement of urinary mono hydroxy polycyclic aromatic hydrocarbons using automated liquid-liquid extraction and gas chromatography/isotope dilution high-resolution mass spectrometry, *Anal. Chem.*, 78 (2006) 5744–5751.
- [9] M. Rezaee, Y. Assadi, M.R.M. Hosseini, E. Aghae, F. Ahmadi, S. Berijani, Determination of organic compounds in water using dispersive liquid-liquid microextraction, *J. Chromatogr. A*, 1116 (2006) 1–9.
- [10] H. Bagheri, E. Babanezhad, A. Eshaghi, An aniline-based fiber coating for solid phase microextraction of polycyclic aromatic hydrocarbons from water followed by gas chromatography-mass spectrometry, *J. Chromatogr. A*, 1152 (2007) 168–174.
- [11] J.N. Bianchin, G. Nardini, J. Merib, A.N. Dias, E. Martendal, E. Carasek, Simultaneous determination of polycyclic aromatic hydrocarbons and benzene, toluene, ethylbenzene and xylene in water samples using a new sampling strategy combining different extraction modes and temperatures in a single extraction solid-phase microextraction-gas chromatography-mass spectrometry procedure, *J. Chromatogr. A*, 1233 (2012) 22–29.
- [12] T. Wang, M. Guo, W. Song, Y. Zhang, X. Du, A new nitrogen-containing carbon nanoparticle coated stainless steel fiber for selective solid-phase microextraction of ultraviolet filters, *Anal. Methods*, 7 (2015) 3385–3394.
- [13] G. Zhang, X. Zang, Z. Li, C. Wang, Z. Wang, Polydimethyl siloxane/metal-organic frameworks coated fiber for solid-phase microextraction of polycyclic aromatic hydrocarbons in river and lake water samples, *Talanta*, 129 (2014) 600–605.
- [14] Sh.X. Gong, X. Wang, Y. Chen, Ch.G. Cheng, M. Lin Wang, R.S. Zhao, Carboxylated solid carbon spheres as a novel solid-phase microextraction coating for sensitive determination of phenols in environmental water samples, *J. Chromatogr. A*, 1401 (2015) 17–23.
- [15] J. Feng, M. Sun, L. Li, X. Wang, H. Duan, C. Luo, Multiwalled carbon nanotubes-doped polymeric ionic liquids coating for multiple headspace solid-phase microextraction, *Talanta*, 123 (2014) 18–24.
- [16] W. Du, F. Zhao, B. Zeng, Novel multiwalled carbon nanotubes-polyaniline composite film coated platinum wire for headspace solid-phase microextraction and gas chromatographic determination of phenolic compounds, *J. Chromatogr. A*, 1216 (2009) 3751–3757.
- [17] A. Mehdinia, H. Khani, S. Mozaffari, Fibers coated with a graphene-polyaniline nanocomposite for the headspace solid-phase microextraction of organochlorine pesticides from seawater samples, *Microchim. Acta*, 181 (2014) 89–95.

- [18] M.M. Abolghasemi, B. Karimi, V. Yousefi, Periodic mesoporous organosilica with ionic liquid framework as a novel fiber coating for headspace solid-phase microextraction of polycyclic aromatic hydrocarbons, *Anal. Chim. Acta*, 804 (2013) 280–286.
- [19] D. Djozan, B. Ebrahimi, Preparation of new solid phase microextraction fiber on the basis of atrazine-molecular imprinted polymer: application for GC and GC/MS screening of triazine herbicides in water, rice and onion, *Anal. Chim. Acta*, 616 (2008) 152–159.
- [20] X. Hou, Y. Guo, X. Liang, X. Wang, L. Wang, L. Wang, X. Liu, Bis(trifluoromethanesulfonyl) imide- based ionic liquids grafted on graphene oxide-coated solid-phase microextraction fiber for extraction and enrichment of polycyclic aromatic hydrocarbons in potatoes and phthalate esters in food-wrap, *Talanta*, 153 (2016) 392–400.
- [21] H. Hu, S. Liu, C. Chen, J. Wang, Y. Zou, L. Lin, S. Yao, Two novel zeolitic imidazolate frameworks (ZIFs) as sorbents for solid-phase extraction (SPE) of polycyclic aromatic hydrocarbons (PAHs) in environmental water samples, *Analyst*, 139 (2014) 5818–5826.
- [22] S.-H. Huo, X.-P. Yan, Facile magnetization of metal-organic framework MIL-101 for magnetic solid-phase extraction of polycyclic aromatic hydrocarbons in environmental water samples, *Analyst*, 137 (2012) 3445–3451.
- [23] W. Li, Y. Zhang, Q. Li, G. Zhang, Metal-organic framework composite membranes: synthesis and separation applications, *Chem. Eng. Sci.*, 135 (2015) 232–257.
- [24] T. Han, Y. Xiao, M. Tong, H. Huang, D. Liu, L. Wang, C. Zhong, Synthesis of CNT@MIL-68(Al) composites with improved adsorption capacity for phenol in aqueous solution, *Chem. Eng. J.*, 275 (2015) 134–141.
- [25] S. Paulose, R. Raghavan, B.K. George, Graphite oxide-iron oxide nanocomposites as a new class of catalyst for the thermal decomposition of ammonium perchlorate, *RSC Adv.*, 6 (2016) 45977–45985.
- [26] B.C. Petit, T.J. Bandoz, Enhanced adsorption of ammonia on metal-organic framework/graphite oxide composites: analysis of surface interactions, *Adv. Funct. Mater.*, 20 (2010) 111–118.
- [27] S. Su, B. Chen, M. He, B. Hu, Graphene oxide-silica composite coating hollow fiber solid phase microextraction online coupled with inductively coupled plasma mass spectrometry for the determination of trace heavy metals in environmental water samples, *Talanta*, 123 (2014) 1–9.
- [28] M. Ahmadvand, H. Sereshti, H. Parastar, Chemometric-based determination of polycyclic aromatic hydrocarbons in aqueous samples using ultrasound-assisted emulsification microextraction combined to gas chromatography-mass spectrometry, *J. Chromatogr. A*, 1413 (2015) 117–126.
- [29] L. Zhao, Q. Li, X. Xu, W. Kong, X. Li, Y. Su, Q. Yue, B. Gao, A novel enteromorpha based hydrogel optimized with Box-Behnken response surface method: synthesis, characterization and swelling behaviors, *Chem. Eng. J.*, 287 (2016) 537–544.
- [30] Z. Chen, F. Dong, S. Li, Z. Zheng, Y. Xu, J. Xu, X. Liu, Y. Zheng, Response surface methodology for the enantioseparation of dinotefuran and its chiral metabolite in bee products and environmental samples by supercritical fluid chromatography/tandem mass spectrometry, *J. Chromatogr. A*, 1410 (2015) 181–189.
- [31] X. Hou, S. Liu, P. Zhou, J. Li, X. Liu, L. Wang, Y. Guo, Polymeric ionic liquid modified graphene oxide-grafted silica for solid-phase extraction to analyze the excretion-dynamics of flavonoids in urine by Box-Behnken statistical design, *J. Chromatogr. A*, 1456 (2016) 10–18.
- [32] J. Chen, B. Yao, C. Li, G. Shi, An improved Hummers method for eco-friendly synthesis of graphene oxide, *Carbon*, 64 (2013) 225–229.
- [33] S. Zhang, Z. Du, G. Li, Metal-organic framework-199/graphite oxide hybrid composites coated solid-phase microextraction fibers coupled with gas chromatography for determination of organochlorine pesticides from complicated samples, *Talanta*, 115 (2013) 32–39.
- [34] G. Vas, K. Vekey, Solid-phase microextraction: a powerful sample preparation tool prior to mass spectrometric analysis, *J. Mass Spectrom.*, 39 (2004) 233–254.
- [35] Y. Wang, Y. Wu, H. Ge, H. Chen, G. Ye, X. Hu, Fabrication of metal-organic frameworks and graphite oxide hybrid composites for solid-phase extraction and preconcentration of luteolin, *Talanta*, 122 (2014) 91–96.
- [36] D. Konios, M.M. Stylianakis, E. Stratakis, E. Kymakis, Dispersion behaviour of graphene oxide and reduced graphene oxide, *J. Colloid Interface Sci.*, 430 (2014) 108–112.
- [37] Q. Zhou, Y. Gao, Determination of polycyclic aromatic hydrocarbons in water samples by temperature controlled ionic liquid dispersive liquid-liquid microextraction combined with high performance liquid chromatography, *Anal. Methods*, 6 (2014) 2553–2559.
- [38] J.S. Ribeiro, R.F. Teófilo, F. Augusto, M.M.C. Ferreira, Simultaneous optimization of the microextraction of coffee volatiles using response surface methodology and principal component analysis, *Chemom. Intell. Lab. Syst.*, 102 (2010) 45–52.
- [39] S.L.C. Ferreira, R.E. Bruns, H.S. Ferreira, G.D. Matos, J.M. David, G.C. Brandão, E.G.P. da Silva, L.A. Portugal, P.S. dos Reis, A.S. Souza, W.N.L. dos Santos, Box-Behnken design: an alternative for the optimization of analytical methods, *Anal. Chim. Acta*, 597 (2007) 179–186.
- [40] M. Khajeh, Optimization of process variables for essential oil components from *Satureja hortensis* by supercritical fluid extraction using Box-Behnken experimental design, *J. Supercrit. Fluids*, 55 (2011) 944–948.
- [41] Y. Zheng, Y. Liu, A. Wang, Fast removal of ammonium ion using a hydrogel optimized with response surface methodology, *Chem. Eng. J.*, 171 (2011) 1201–1208.
- [42] K.P. Singh, S. Gupta, A.K. Singh, S. Sinha, Experimental design and response surface modeling for optimization of rhodamine B removal from water by magnetic nanocomposite, *Chem. Eng. J.*, 165 (2010) 151–160.
- [43] S.K. Chakraborty, B.K. Kumbhar, S. Chakraborty, P. Yadav, Influence of processing parameters on textural characteristics and overall acceptability of millet enriched biscuits using response surface methodology, *J. Food Sci. Technol.*, 48 (2011) 167–174.
- [44] N. Alizadeh, H. Zarabadipour, A. Mohammadi, Headspace solid-phase microextraction using an electrochemically deposited dodecylsulfate-doped polypyrrole film to determine of phenolic compounds in water, *Anal. Chim. Acta*, 605 (2007) 159–167.
- [45] H. Bagheri, E. Babanezhad, F. Khalilian, A novel sol-gel-based amino-functionalized fiber for headspace solid-phase microextraction of phenol and chlorophenols from environmental samples, *Anal. Chim. Acta*, 616 (2008) 49–55.
- [46] A.N. Dias, V. Simao, J. Merib, E. Carasek, Cork as a new (green) coating for solid-phase microextraction: determination of polycyclic aromatic hydrocarbons in water samples by gas chromatography-mass spectrometry, *Anal. Chim. Acta*, 772 (2013) 33–39.
- [47] R. Mirzajani, F. Kardani, Fabrication of ciprofloxacin molecular imprinted polymer coating on a stainless steel wire as a selective solid-phase microextraction fiber for sensitive determination of fluoroquinolones in biological fluids and tablet formulation using HPLC-UV detection, *J. Pharm. Biomed. Anal.*, 122 (2016) 98–109.
- [48] M. Guo, W. Song, T. Wang, Y. Li, X. Wang, X. Du, Phenyl-functionalization of titanium dioxide-nanosheets coating fabricated on a titanium wire for selective solid-phase microextraction of polycyclic aromatic hydrocarbons from environment water samples, *Talanta*, 144 (2015) 998–1006.
- [49] J. Fan, Z. Dong, M. Qi, R. Fu, L. Qu, Monolithic Graphene fibers for solid-phase microextraction, *J. Chromatogr. A*, 1320 (2013) 27–32.
- [50] L. Xu, J. Feng, J. Li, X. Liu, S. Jian, Graphene oxide bonded fused-silica fiber for solid-phase microextraction-gas chromatography of polycyclic aromatic hydrocarbons in water, *J. Sep. Sci.*, 35 (2012) 93–100.

- [51] M. Sun, J. Feng, Y. Bu, C. Luo, Highly sensitive copper fiber-in-tube solid-phase microextraction for online selective analysis of polycyclic aromatic hydrocarbons coupled with high performance liquid chromatography, *J. Chromatogr. A*, 1408 (2015) 41–48.
- [52] Q.L. Li, X. Wang, X.F. Chen, M.L. Wang, R.S. Zhao, In situ hydrothermal growth of ytterbium-based metal-organic framework on stainless steel wire for solid-phase microextraction of polycyclic aromatic hydrocarbons from environmental samples, *J. Chromatogr. A*, 1415 (2015) 11–19.
- [53] A.A. Matin, P. Biparva, M. Gheslagh, Gas chromatographic determination of polycyclic aromatic hydrocarbons in water and smoked rice samples after solid-phase microextraction using multiwalled carbon nanotube loaded hollow fiber, *J. Chromatogr. A*, 1374 (2014) 50–57.

Supplementary information

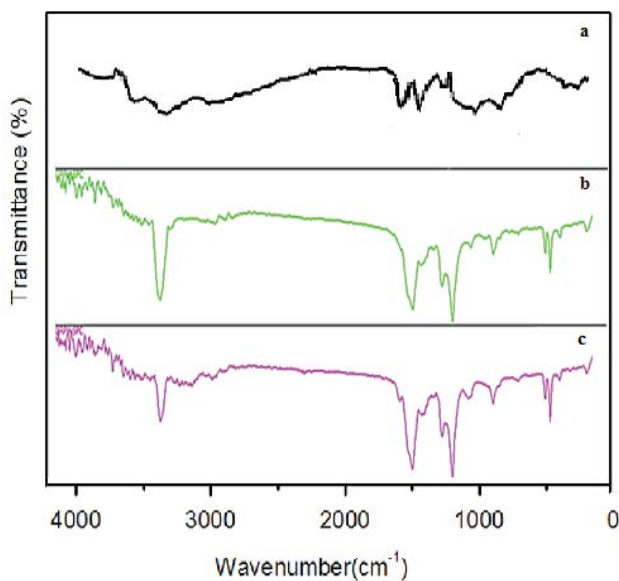


Fig. S1. FTIR spectra of (a) GO, (b) Cu₃(BTC)₂, and (c) Cu₃(BTC)₂/GO.

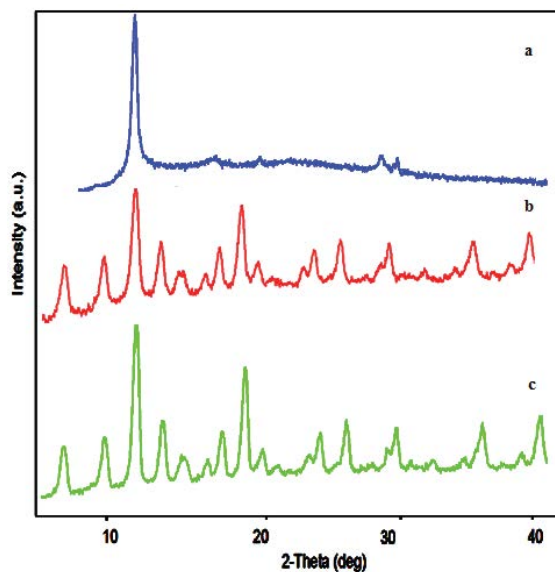


Fig. S2. X-ray diffraction patterns of (a) GO, (b) Cu₃(BTC)₂, and (c) Cu₃(BTC)₂/GO.

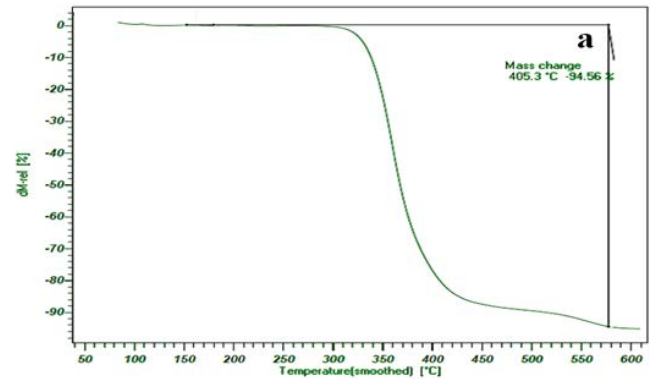


Fig. S3. TGA thermographs of Cu₃(BTC)₂/GO nanocomposite coating.